Field-Flood Requirements for Emission Computed Tomography with an Anger Camera

W. L. Rogers, N. H. Clinthorne, B. A. Harkness, K. F. Koral, and J. W. Keyes, Jr.

University of Michigan Medical Center, Ann Arbor, Michigan

Emission computed tomography with a rotating camera places stringent requirements on camera uniformity and the stability of camera response. In terms of clinical tomographic imaging, we have studied the statistical accuracy required for camera flood correction, the requirements for flood accuracy, the utility and validity of flood and data image smoothing to reduce random noise effects, and the magnitude and effect of camera variations as a function of angular position, energy window, and tuning. Uniformity of the corrected flood response must be held to better than 1% to eliminate image artifacts that are apparent in a million-count image of a liver slice. This requires calibration with an accurate, well-mixed flood source. Both random fluctuations and variations in camera response with rotation must be kept below 1%. To meet the statistical limit, one requires at least 30 million counts for the flood-correction image. Smoothing the flood image alone introduces unacceptable image artifacts. Smoothing both the flood image and data, however, appears to be a good approach toward reducing noise effects. Careful camera tuning and magnetic shield design provide camera stability suitable for present clinical applications.

With the advent of commercial Anger-camera systems for emission tomography, it has become exceedingly important to appreciate how critical camera uniformity is for good imaging, and to understand the factors that must be controlled to ensure appropriate camera performance. Several authors have described the effects of detector nonuniformity on reconstructed images for both transmission and emission tomography (1–5). The reconstruction algorithms greatly amplify the effects of camera nonuniformity. Amplification depends inversely on the square root of the defect's distance from the center of rotation of the tomograph for r ≫ 0, and directly on the diameter of the source distribution being imaged (2,4). Amplification is also governed by the relationship between the spatial frequency components of the defect and the reconstruction filter.

As an illustration of the severity of the problem, images of uniform cylinders 31 and 51 pixels in diameter were reconstructed from computer-generated projections containing a 2% Gaussian defect with FWHM of 4 pixels. The reconstructed images exhibited 10% and 15% defects, respectively. These results were observed with the defect located at the center of rotation for a hanning-windowed reconstruction filter with a cutoff equal to 32 cycles per 64-pixel image width. This means that even in the case of relatively smooth defects, camera uniformity must be corrected to about 0.5% in order to keep image distortion under 5% for objects between 20 and 30 cm in diameter.

Nonuniform flood response of a camera can be attributed to nonuniform point-source sensitivity, to spatial distortion, or to a combination of both (6,7). As long as spatial distortion is small, it does not appear to contribute

significantly to image degradation if the nonuniform flood response is corrected by performing a conventional, multiplicative flood correction of the data (*4*):

$$f_i = \text{mean flood counts}/c_i, \qquad (1)$$

where the correction factor for the *i*th image element is f_i and c_i is the number of counts in the *i*th pixel of the flood image.

In this paper, we report an investigation into the practical steps that must be taken to achieve a satisfactory flood correction for tomographic imaging. In particular, we address the following questions:

1. Are conventional radioactive flood sources sufficiently uniform?
2. What statistical accuracy is required for the flood-calibration image?
3. Can the flood-calibration image be smoothed to reduce random noise?
4. What is the camera's flood response as a function of angular position and energy window? Is it sufficiently constant to permit a conventional flood correction?

METHODS

In order to provide a reliable calibration standard, a precision flood source was constructed. A source cavity 17 in. in diameter was machined in a 1.25-in.-thick cast aluminum tooling plate to a depth of 1.00 in. with a tolerance of ±0.002 in. A half-inch thick plexiglass cover, also machined to ±0.002 in., was fastened to the body of the phantom with urethane adhesive. These tolerances ensure that the source uniformity is within 0.5% if the filling liquid is properly mixed. The aluminum body ensures rigidity of the phantom, while the plastic cover allows one to verify that no air bubbles are included. To prevent the plexiglass window from bulging, the phantom is filled while clamped to a flat plate. After filling, the phantom is thoroughly mixed with a magnetic stirrer. When the phantom is in use, the stirring bar is stored in the filling channel out of the field of view.

The uniformity of a commercial flood source was determined by acquiring a 120-million-count precision flood-calibration image, and a 120-million-count image of the commercial flood source. No attempt was made to flatten the commercial source, but it was thoroughly mixed and all air bubbles were excluded. The image of the commercial flood was corrected for camera nonuniformity with the precision flood and examined for residual structure intrinsic to the source itself. The effect of this source's structure on tomographic reconstruction was evaluated using computer-generated projection data for a cylinder 41 pixels in diameter with an assumed camera resolution of 1.5 cm FWHM. The synthetic projection data were multiplied by correction coefficients calculated from the corrected commercial flood image.

Tomographic images were reconstructed using a convolution back-projection algorithm that used a ramp filter multiplied by a hanning window with a cutoff frequency of 32 cycles per picture width. Both the projections and the reconstructed images were 64 elements wide.

Image artifacts contributed by random noise in the calibration flood image were also studied using the simulated-cylinder projection data. Both noisy and noise-free cylinder data were used. Synthetic floods with a uniform mean distribution and varying amounts of pseudorandom Gaussian noise were computer generated and used to "correct" the simulated-cylinder projection data. Again, several tomographic slices were reconstructed and the amplitude and appearance of the image artifacts propagated from the noisy simulated flood were noted. Next, the simulated noisy floods were preprocessed by a nine-point smooth or by a 3 × 3 median filter to reduce the random fluctuations. These processed floods were used to correct the simulated-cylinder data as above, and two new sets of tomographic images were reconstructed for comparison with the first.

Since the simulated flood is uniform, smoothing will not alter the mean spatial distribution, but an experimental flood image can contain significant structure that depends upon the specific camera and its state of tuning. If the flood response does contain defects with high spatial frequency, smoothing will introduce deterministic errors in the correction coefficients, as described in the Appendix. To examine this problem for the specific case of the rotating Anger camera tomograph in our laboratory,* an experimental 120-million-count precision flood-source image was acquired. A smoothed image of the experimental flood was then multiplied by correction coefficients calculated from the unsmoothed flood data. These corrected flood images then contain only the deterministic errors introduced by the smoothing, plus random noise. The propagation of these errors through the reconstruction algorithm was determined by using the corrected, smoothed floods to correct in turn the simulated-cylinder data before reconstruction of a series of transverse-section images.

A second approach toward reducing the effect of random error in the flood-calibration image is to smooth both the flood and the data with the same smoothing function. From Eq. (10) in the Appendix, it is evident that if the detector efficiency function $\bar{\epsilon}(x,y)$ is a constant, it may be removed from the convolution integral and no deterministic error will be introduced. It is necessary, therefore, to test whether noticeable artifacts are generated in the experimental case where $\bar{\epsilon}(x,y)$ is nonuniform. Data were acquired from a Tc-99m-filled cylinder phantom 17 cm in diameter and 25.5 cm long, containing an 18-mm-diameter defect without radioactivity. The projection images were singly and doubly smoothed with a nine-point kernel and flood corrected
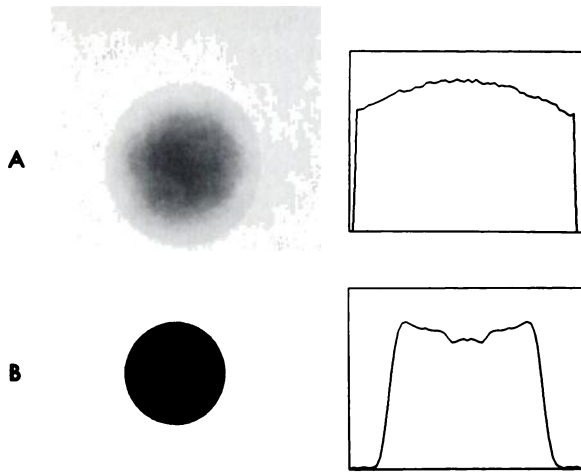
FIG. 1. (A) Image (120 × 10⁶ counts) and central profile of conventional flood source, corrected for camera nonuniformity with a 120-million-count precision-flood image. Center of profile is 25% higher than edges. (B) Transverse-section image of synthetic cylinder with data corrected using flood image a. Center point of cylinder is 12% below outside edge.

with the 120-million count precision flood that had been identically smoothed. The reconstructed images were visually examined for artifacts resulting from the smoothing.

The final task, that of determining the dependence of the flood response on camera orientation, was accomplished by clamping a flood source to the collimator face and acquiring images for several rotational positions of the camera head. Significant changes in the flood images were observed. To eliminate the possibility that the flood source was distorting under its own weight and to determine whether the observed changes were caused by interaction with the earth's magnetic field or by gravitational deformation of the phototubes' dynode structures, all further measurements were obtained with the camera facing up and rotated azimuthally on its base. Thirty-million-count flood images were obtained with the camera gantry pointing east, south, and west. The first measurement was repeated and used to flood correct the other three images. Structure in these corrected images, occurring as a function of camera gantry orientation, was then examined in high-contrast images, and variation in the count rate for 3 × 3 pixel regions of interest along the tomographic axis of rotation were plotted as a function of azimuthal angle. Pulse-height spectra were also obtained from several individual phototubes for various camera orientations.

Sensitivity of the camera to orientation changes was examined as a function of camera tuning, magnetic shielding, and energy-window setting. Two different criteria were used to tune the camera:

(a) uniform point-source response;
(b) equal phototube gain.

Measurements were made with inadequate magnetic

shielding and with prototype shielding designed by the manufacturer specifically for tomography. Energy windows of 15%, 20%, and 30% were investigated.

Spatial distortion and its dependence on camera position were determined by imaging an orthogonal hole phantom at the same azimuthal angles described above. Maximum and mean departures from camera linearity at each angle were determined by fitting the hole pattern with an orthogonal grid (8).

RESULTS

Figure 1 shows a 120-million-count image of a conventional flood source with the image corrected using the precision flood-source image. The central profile shows a smooth 25% bulge in the flood source, which appears in the reconstructed image as a 12% dip. The fine structure exhibits a relative standard deviation (RSD) of 0.7% from the smooth curve. This is precisely the RSD to be expected from using a flood image with a 0.5% RSD to correct a second flood with the same random error. This error shows up as ring structure in the reconstructed slices and is addressed below.

Figure 2 illustrates reconstructed slices of the simulated cylinder corresponding to relative standard deviations of 0.5%, 1%, and 2% in the synthetic flood data. The artifact amplitudes in the reconstructed slice for these three cases are 3%, 6%, and 12%, respectively. The ring patterns are identical since in each case the same pseudorandom sequence is used to generate the noise, and only the amplitude is changed. The illustrated slices are only representative. For example, other slices for the 1% noise simulation show defects with amplitudes
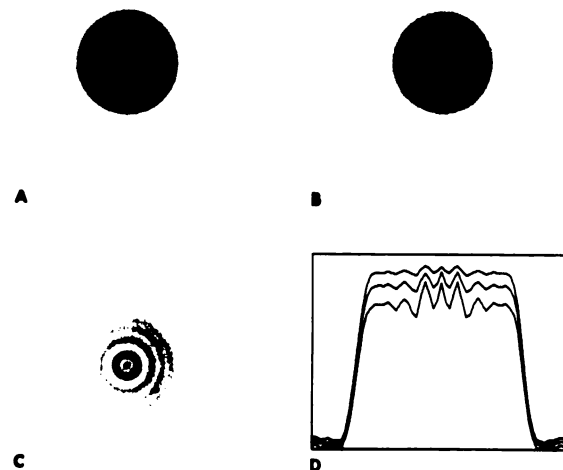
FIG. 2. Effect of random noise in calibration flood image on reconstructed-cylinder images. Standard deviations in flood image are: (A) 0.5%, (B) 1%, (C) 2%. Central profiles shown in (D) are offset to separate curves.
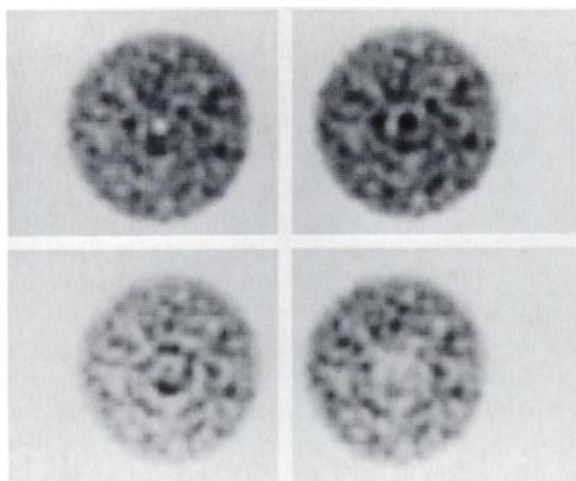
FIG. 3. Illustrations of artifacts due to flood noise still evident despite presence of image noise. Four selected slices of 41-pixel diameter cylinder reconstructed from 2.5 × 10⁶ counts per slice simulated data. Simulated flood used for correction contained noise with 1% relative standard deviation.

FIG. 4. Effect of smoothing an experimentally acquired flood from commercial tomograph. Transverse-section image of cylinder reconstructed from simulated data corrected with: (A) unsmoothed flood, (B) singly smoothed flood, (C) doubly smoothed flood. Profiles (D) as in Fig. 2.

ranging from −22% to +30% arising from the extremes in the noise distribution.

The synthetic flood with 1% RSD was also used to correct cylinder data to which noise had been added, so that we could determine to what extent image noise masked the correction-noise artifacts. For a noise level simulating 1 million counts per slice in the 41-pixel cylinder (25 cm diam), the ring artifacts were virtually undetectable in the reconstructions. However, when the count density was increased to 2.5 million per slice, the artifacts were readily apparent, as illustrated in Fig. 3.

Smoothing and median filtering of the synthetic flood image effectively reduced the artifacts in the reconstructed image caused by flood-noise fluctuations. A single nine-point smoothing reduced the image variation by a factor of 2. Median filtering was less effective in that some high frequency structure was preserved. The problem with smoothing only the floods to reduce the random noise is that the technique cannot be applied to experimentally obtained flood data because the smoothed correction factors can no longer correct for camera defects with high spatial frequency. This problem is discussed in the Appendix and is illustrated in Fig. 4, which shows synthetic-cylinder reconstructions corrected with factors derived from an unsmoothed real flood, a singly smoothed real flood, and a doubly smoothed real flood. Errors of 8.5% and 17% are produced by single and double smoothing, respectively.

Figure 5 shows high-contrast images of the camera flood taken with the camera gantry pointing south and west. These images have been corrected using a flood image acquired when the camera gantry was pointing east, so that all visible structure is due solely to changes in camera response with angle. In all cases, the energy
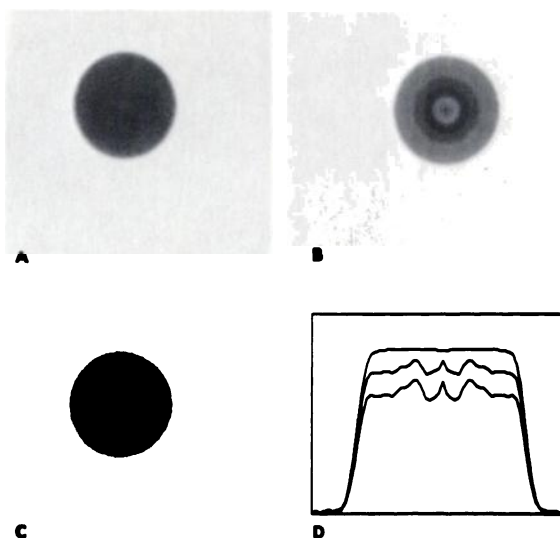
window was 20%, and the camera was tuned for equal gain. The upper two images were acquired with inadequate magnetic shielding; the lower two with the new prototype shielding. Evaluation of the regional count-rate variation as a function of azimuthal position for the two cases illustrated in Fig. 5 shows a reduction from ±5.5% to about ±1% when the prototype shielding is added.

Pulse-height spectra measured for single phototubes showed a 1–2% shift in peak position as the unshielded
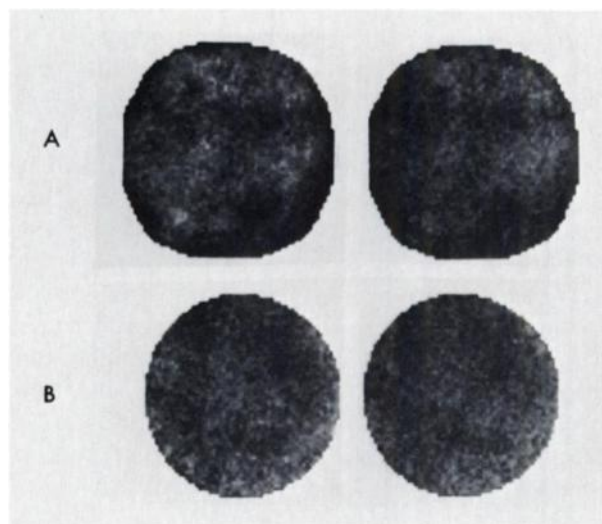
FIG. 5. Flood images from a commercial tomograph* acquired at two different camera gantry orientations and flood corrected with data acquired with camera gantry pointed east. (A) Camera magnetic shielding inadequate; (B) improved magnetic shielding. In both A and B, image contrast is enhanced a factor of 5.
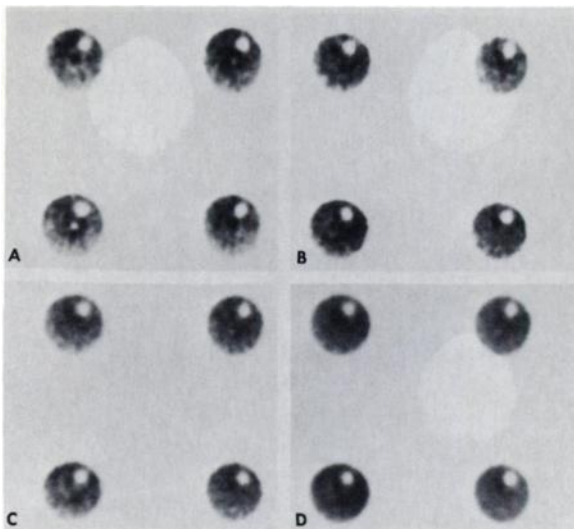
FIG. 6. Reconstructions of data from experimental cylinder phantom. Four worst slices are shown, each containing 10⁶ counts. (A) Inadequate magnetic shielding, 30-million-count conventional flood. (B) Improved magnetic shielding 120-million-count precision flood. (C) Same data and slices as in B except flood and projection data smoothed. (D) Same as in C except double smooth used.

camera was rotated azimuthally on its base from east to west. The corresponding count-rate variation depended on peak shape, window width, and whether or not the peak was centered in the window. When count rates for 3 × 3 regions of interest in the flood image were plotted as a function of camera rotation, 12% changes were observed for a 15% window when the camera had been tuned to give uniform point-source sensitivity. Retuning the camera to align all the photopeaks in the window reduced the maximum variation with angle to about 7%. Increasing the window to 20% and 30% further reduced the peak variation to 5.5% and 3.1%, respectively.

Measurements of spatial distortion made on the camera with improved shielding showed a maximum vector distortion of 5 mm. Over a central region 26 cm in diameter, the maximum distortion was 2 mm, or ⅓ pixel. No measurable angular dependence was detected.

Figure 6 compares four sets of high-contrast transverse-section images of the Tc-99m-filled cylinder phantom to illustrate the overall improvement in image quality achieved with suitable magnetic shielding and precision flood correction, together with combined smoothing of the projection data and flood image. An energy window of 20% was used and the images contain 1 million counts per slice. From a total of 30 reconstructed slices, the four worst images were selected in each case. Data for the first set of images, Fig. 6(A), were acquired with inadequate magnetic shielding and were flood corrected using a 30-million-count conventional flood image. These images display a prominent ring structure, with central defects that vary from −24%

to +20%. Data for the second set of images, Fig. 6(B), were acquired with improved magnetic shielding and were corrected with a 120-million-count precision flood image. Figure 6(C,D) are the same slices, reconstructed from the same data as Fig. 6(B) but after single and double smoothing of the flood image and projection data. These images were reconstructed with a straight ramp filter to avoid additional smoothing.

In Fig. 6(B), only the fourth slice contains, at the center of rotation, a focal area of radioactivity that appears to exceed expected random noise. This area persists in the smoothed images, suggesting that it is not due to noise. In addition, as the random noise is reduced by smoothing, the third slice begins to show a faint arc about the center of rotation. These artifacts are most likely to arise from residual variation in angular sensitivity of the camera. The magnitude of this residual artifact was quantified by determining the peak variations (max-min) divided by the mean and the relative standard deviations for regions of interest at the center of rotation and at the perimeter of 30 serial sections of the cylinder, for which the data and flood images were singly smoothed. The relative standard deviation was 2.3% at the center of rotation and 1.6% at the perimeter. The corresponding peak variations were 8.2% and 4.8%. These differences support the hypothesis that there is residual camera variation because defects at the center of rotation are amplified most during reconstruction. Since no defect appears common to all slices, smoothing both the flood image and the data appears valid for the cylindrical phantom. The validity of this approach for other objects remains to be proven.

DISCUSSION

Amplification of error by the tomographic reconstruction algorithm imposes an increase in uniformity and stability requirements of almost an order of magnitude on the Anger camera for tomographic use as compared to conventional imaging. The most severe requirements are placed on regions along the axis of rotation, where even relatively broad Gaussian defects can be amplified by a factor of 10 or more depending on object size.

The defect magnitude that can be tolerated is related to the amount of noise in the data. For instance, the 2.5 × 10⁶ count, 41-pixel diameter, cylinder sections show detectable artifacts with only 1% noise in the flood image. By using Budinger's (9) signal-to-noise estimate for uniform cylinders, 2.5 × 10⁶ counts in a 41-pixel cylinder will give about the same signal-to-noise ratio as 1 million counts in a 31-pixel cylinder, the latter containing roughly the same number of pixels as a liver section. The liver image is probably the most critical clinical test for the detection of artifacts because it is a large, relatively uniform object generally overlying the

center of rotation. Since a liver image with 1 million counts per slice is the norm at our institution, it is necessary to keep camera-correction errors under 1%. This refers mainly to high-spatial-frequency defects such as intrinsic camera defects and random noise in the calibration flood. The error introduced by the gradual bulge in the commercial calibration phantom is of less consequence, and could be largely eliminated by clamping the phantom between two flat plates during filling.

Imposing greater than 1% statistical accuracy on the flood image means acquiring flood images with at least 30 million counts. At reasonable count rates, a 30-million-count image requires 20–30 min. Increasing the accuracy to 0.5% increases the acquisition time a factor of 4, which is prohibitive. We have demonstrated experimentally with one commercial instrument that smoothing the flood alone creates worse defects than noise in the flood image. Equation (6) in the Appendix shows that this deterministic error is related only to the ratio of the unsmoothed to the smoothed detector efficiency function. This error is constant for all projections, and therefore contributes highly structured defects in the image whose amplitude will vary inversely as the square root of the defect distance from the center of rotation. On the other hand, if both the flood image and projection data are smoothed with the same function, the deterministic error shown in Eq. (10) of the Appendix is a function of each given projection, and therefore will not generally create highly structured defects with an inverse radial dependence. Indeed, our experimental images of a cylindrical phantom showed no evidence of defects from this smoothing. If the projection is smooth compared with the smoothing function, it is shown that the error theoretically vanishes.

The question of calibration for different nuclides has not been addressed. In view of the sensitivity of camera response to slight changes in phototube gain and photopeak shape, it seems a poor practice to correct thallium images with a technetium flood. However, thallium flood images could be obtained economically only with a point source and no collimator. In this event, the collimator response would need to be measured once and stored so it could be incorporated into the intrinsic camera flood response. Perhaps the saving grace is that the heart is a small organ and generally does not lie at the center of rotation so that uniformity artifacts are not very apparent.

Use of cobalt flood sources for camera calibration has not been examined either. Commercial cobalt flood sources are only guaranteed to be uniform to within ±4% for regions 2.5 in cm diameter. The size and shape of nonuniformities are not specified. The fact that better than 1% uniformity is necessary for calibration, together with the fact that the cobalt gamma ray is 14% lower in energy than that of Tc-99m suggests that Co-57 calibration should be carefully studied before it is used. The

uniformity of any given source must be established and the camera's response to cobalt at its window setting and to Tc-99m at its window setting must be shown to be identical to within 1%.

With appropriate attention to camera tuning and magnetic shielding, it is possible to reduce camera variation with rotation to the 1% level. These changes have a sinusoidal shape and, therefore, show up in the images as arcs rather than as complete rings. As such, they tend to be more easily masked by image noise. One-percent camera variations do not contribute detectable structure in images of a cylinder 19 cm in diameter and containing 1 million counts per slice. Since this approximates clinical liver imaging, the worst clinical case, it seems that 1% camera variation is acceptable for clinical imaging.

If smoothing of flood and clinical images is used to reduce the effect of noise, it is possible that residual camera variations of less than 1% could cause visible artifacts. In our experiments with smoothing, some structure did become apparent in a few of the reconstructed slices of the cylinder phantom [Fig. 6(C,D)]. In this particular case, the relative standard deviation and peak variations at the center of rotation exceeded those at the edge by only 0.7% and 3.4%, respectively. This still seems acceptable for clinical imaging.

CONCLUSIONS AND RECOMMENDATIONS

Tomography places extremely stringent requirements on Anger-camera performance and correction techniques. Flood normalization requires an accurate, well-mixed flood source with random variation less than 1%. Pains should be taken to remove the bulge from conventional liquid sources. On the basis of guaranteed uniformity and difference in energy, Co-57 flood sources appear inferior to liquid-filled Tc-99m sources. Thirty-million-count flood calibrations are recommended.

Smoothing the flood image alone in order to reduce random noise introduces unacceptable defects in the image. Smoothing both the data and the flood can potentially introduce artifacts, but both experimentally and theoretically these do not appear to be of a serious nature. Since the potential error is object dependent, such smoothing should be examined on a case-by-case basis.

In our experience, careful shielding and camera tuning renders stability adequate for the present clinical applications. Since instrument-to-instrument variations are to be expected and since magnetic field strength can vary depending on building construction and nearby equipment, dependence on camera orientation should be measured for any given installation.

Finally, we suggest that a large uniform cylindrical phantom with a diameter about 2/3 that of the field of view should be used for sensitive testing of overall per-

formance. In a phantom of this diameter, 2.5×10^6 counts per slice will give noise approximating that in a clinical liver image. Increasing the counting statistics until image artifacts are visible will give some idea of the margin of safety for clinical imaging.

FOOTNOTE

* General Electric Company model 400-T with 37 phototube head.

ACKNOWLEDGMENTS

APPENDIX

In order to understand the problems encountered in smoothing the calibration flood image with or without smoothing the data, we examine the correction process analytically. Let $\hat{e}(x,y)$ be an estimate of the detector efficiency function $\bar{e}(x,y)$. If $\hat{I}(x,y)$ is the image obtained with a perfectly uniform detector, a real image $\hat{R}$ (x,y) may be expressed as

$$\hat{R}(x,y) = \hat{I}(x,y) \cdot \bar{e}(x,y). \tag{1}$$

Flood correction is accomplished by dividing Eq. (1) by a noisy estimate of the efficiency function $\hat{e}(x,y)$.

$$\hat{I}'(x,y) = \hat{I}(x,y) \cdot \frac{\bar{e}(x,y)}{\hat{e}(x,y)}. \tag{2}$$

Dropping the explicit arguments x and y and representing the noisy estimates $\hat{I}$ and $\hat{e}$ in terms of the mean values plus a noise term, we obtain

$$\hat{I}' = (\bar{I} + \delta I) \cdot \frac{\bar{e}}{\bar{e} + \delta e}. \tag{3}$$

Expanding the denominator, we obtain

$$\hat{I}' = (\bar{I} + \delta I) \cdot (1 - \delta e/\bar{e} + \cdots). \tag{4}$$

As the noise in the calibration image, δe, approaches 0, $\hat{I}'$ approaches the image that would be obtained with a perfectly uniform camera. Now consider what happens if $\hat{e}$ is convolved with a smoothing function S:

$$\hat{I}' = (\bar{I} + \delta I) \cdot \frac{\bar{e}}{S * (\bar{e} + \delta e)}. \tag{5}$$

Again, expanding the denominator we arrive at

$$\hat{I}' = (\bar{I} + \delta I) \cdot \frac{\bar{e}}{S * \bar{e}} \left(1 - \frac{S * \delta e}{S * \bar{e}} + \cdots\right). \tag{6}$$

The deterministic error is given by the ratio of $\bar{e}$ to the smoothed $\bar{e}$. Now if S is a normalized, symmetric function strongly peaked compared with $\bar{e}$, then $\bar{e}$ may be taken out of the convolution integral:

$$\hat{I}' = (\bar{I} + \delta I) \cdot (1 - S * \delta e/\bar{e}). \tag{7}$$

With this approximation, Eq. (7) gives an identical answer to Eq. (4) except that the noise amplitude has been reduced by smoothing. This approximation was valid for the simulated uniform flood, but

not for the experimental flood obtained from the commercial tomograph.

This same formalism can be extended to describe what happens if both the data and calibration flood are smoothed with the same function:

$$\hat{I}' = S * [(\bar{I} + \delta I) \cdot \bar{e}] \cdot \frac{1}{S * (\bar{e} + \delta e)}. \tag{8}$$

Expanding the denominator, we obtain

$$\hat{I}' = S * [\bar{I} \cdot \bar{e} + \delta I \cdot \bar{e}] \cdot \frac{1}{S * \bar{e}} \left(1 - \frac{S * \delta e}{S * \bar{e}} + \cdots\right). \tag{9}$$

Since $\delta e/\bar{e}$ is on the order of 1% for a 30-million-count flood and smoothing will further reduce the relative error, the second-order term can be dropped:

$$\hat{I}' = S * [\bar{I} \cdot \bar{e}] \cdot \frac{1}{S * \bar{e}} + S * [\delta I \cdot \bar{e}] \cdot \frac{1}{S * \bar{e}}. \tag{10}$$

This states that the corrected image after smoothing both the data and flood images is given approximately by the smoothed mean data divided by the smoothed mean efficiency function plus noise terms.

If S is a peaked function relative to the mean image distribution $\bar{I}, \bar{I}$ may be excluded from the convolution integral to give

$$\hat{I}' = \bar{I} + (S * [\delta I \cdot \bar{e}])/(S * \bar{e}). \tag{11}$$

The resultant image in this case is the mean image plus smoothed error terms.

REFERENCES

1. KOWALSKI G: The influence of fixed errors of a detector array on the reconstruction of objects from their projections. *IEEE Trans Nucl Sci* NS24:2006-2016, 1977

2. SHEPP LA, STEIN JA: Simulated artifacts in computerized x-ray tomography. In *Reconstruction Tomography in Diagnostic Radiology and Nuclear Medicine*. Baltimore, University Park Press, 1977, pp 33-48

3. JASZCZAK RJ, COLEMAN RE: Selected processing techniques for scintillation camera based SPECT systems. In *Single Photon Emission Computed Tomography and Other Selected Computer Topics*. Sorenson JA, Ed. New York, Society of Nuclear Medicine, 1980, pp 45-59

4. TODD-POKROPEK A, ZUROWSKI S, SOUSSALINE F: Nonuniformity and artifact creation in tomography. *J Nucl Med* 21:P38, 1980 (abst)

5. SOUSSALINE F, TODD-POKROPEK AE, ZUROWSKI S, et al: Physical performance of an emission computed tomography system using a rotating conventional gamma camera. *J Nucl Med* 21:P16, 1980 (abst)

6. SOUSSALINE F, TODD-POKROPEK AE, RAYNAUD C: Quantitative studies with the gamma camera: correction for spatial and energy distortion. In Proc. of Vth Int. Conf. on Information Processing in Medical Imaging, Nashville, TN, June 1977, pp 360-375

7. KNOLL GF, BENNETT MC, KORAL KF, et al: Removal of gamma camera nonlinearity and nonuniformities through real-time signal processing. *Proceedings of the Conference on Information Processing in Medical Imaging. INSERM* 88: 187-200, 1979

8. CLINTHORNE NH, ROGERS WL, KORAL KF: A program for quantification of gamma camera spatial linearity. *J Nucl Med* 21:P53, 1980 (abst)

9. BUDINGER TF, GULBERG GT, HUESMAN RH: Emission computed tomography. In *Image Reconstruction From Projections: Implementation and Applications*. Herman GT, Ed. Berlin, Springer-Verlag, 1979, pp 147-246